SCIENTIFIC REPORTS

OPEN

Structural, mechanical, and electronic properties of Rh_2B and RhB_2: first-principles calculations

Received: 02 December 2014
Accepted: 30 March 2015
Published: 30 June 2015

Binhua Chu, Da Li, Fubo Tian, Defang Duan, Xiaojing Sha, Yunzhou Lv, Huadi Zhang, Bingbing Liu & Tian Cui

The crystal structures of Rh_2B and RhB_2 at ambient pressure were explored by using the evolutionary methodology. A monoclinic $P2_1/m$ structure of Rh_2B was predicted and donated as Rh_2B-I, which is energetically much superior to the previously experimentally proposed *Pnma* structure. At the pressure of about 39 GPa, the $P2_1/m$ phase of Rh_2B transforms to the $C2/m$ phases. For RhB_2, a new monoclinic $P2_1/m$ phase was predicted, named as RhB_2-II, it has the same structure type with Rh_2B. Rh_2B-I and RhB_2-II are both mechanically and dynamically stable. They are potential low compressible materials. The analysis of electronic density of states and chemical bonding indicates that the formation of strong and directional covalent B-B and Rh-B bonds in these compounds contribute greatly to their stabilities and high incompressibility.

Superhard materials have attracted considerable attention in both fundamental and technological applications due to their superior mechanical properties such as high melting temperature, high hardness, high electrical and thermal conductivity[1]. Previously, it was generally accepted that the superhard materials are those strongly covalent bonded compounds formed by light elements (B, C, N, and O), such as diamond[2,3], *c*-BN[4], BC_5[5], and BC_2N[6] etc. These superhard materials are easily to form strong three-dimensional covalent bonding networks[7,8]. Although diamond is the known hardest material with a measured hardness at 60–120 GPa, but it reacts easily with iron-based materials. The hardness of cubic boron nitride (*c*-BN) is second only to that of diamond. However, it can be synthesised only under high pressure and high temperature conditions which needs great cost[9]. Therefore, great efforts have been devoted to exploring novel hard and ultra-incompressible materials[10–14]. Recently, it was reported that partially covalent heavy transition metal (TM) boride, carbide, nitride, and oxide are found to be good candidates for superhard materials, such as ReB_2, OsB_2, CrB_4 and WB_4[15–20]. These reports revealed that they all possess high bulk and shear moduli. Because the compounds formed by transition metal and light elements usually possess high valence electron density and directional covalent bonds, and those covalent bonds are strong enough to improve the mechanical properties. Moreover, *d* valence electrons are considered to contribute to the hardness of transition-metal compounds. Further, these materials can be synthesized under lower pressure which leads to the low-cost synthesis condition and this is beneficial to their applications. Therefore, these pioneering studies open up a novel route for the search of novel superhard multifunctional materials.

The borides of rhodium are well known for their high melting temperature and hardness. The measured Vickers hardness of bulk $RhB_{1.1}$ was 7-22.6 GPa, when the loads ranging from 0.49 to 9.81N[21]. Later, the 1.0 μm thick $RhB_{1.1}$ film was studied by X-ray diffraction and it possesses a hardness of 44 GPa[22]. Past studies have identified two stoichiometric compositions: RhB (hexagonal structure, No. 194, $P6_3/mmc$). Wang *et al.* reported that when the pressure exceeds 22 GPa, RhB transforms from hexagonal RhB (anti-NiAs type) to the orthorhombic *Pnma* space group (FeB type)[23], Rh_2B (No.62, *Pnma*) has been determined that it possesses an orthorhombic structure[24]. In 1953, Richard *et al.* studied the crystal structure of Rh_2B from X-ray rotation and Weissenberg photographs. Over the past 60 years,

State Key Laboratory of Superhard Materials, College of physics, Jilin University, Changchun, 130012, P. R. China. Correspondence and requests for materials should be addressed to T.C. (email: cuitian@jlu.edu.cn)

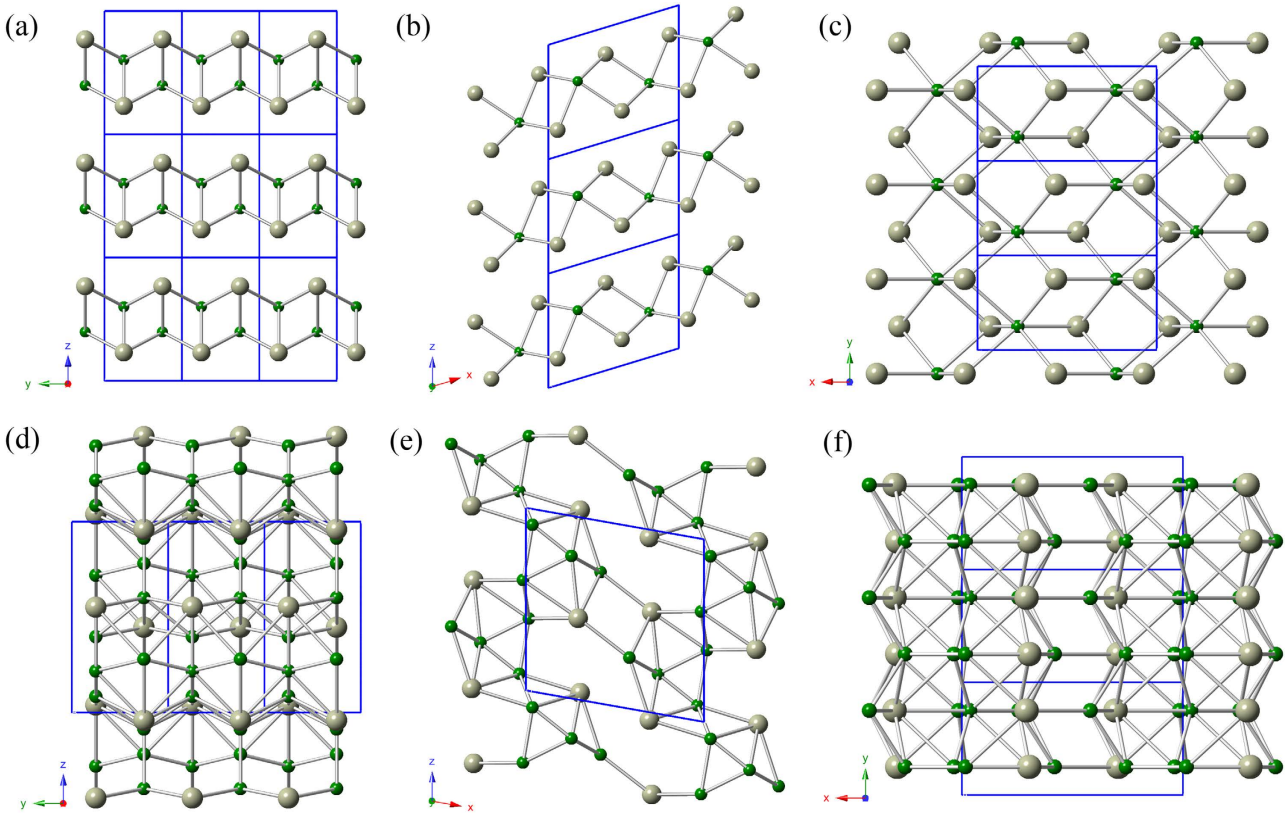

Figure 1. Crystal structures. The green spheres represent the B atoms, and the gray ones represent the Rh atoms. (**a**) (**b**) (**c**) Rh_2B-I and (**d**) (**e**) (**f**) RhB_2-II.

experimental equipment and technology have been improved dramatically, but there is no report about Rh_2B in these years. This led us to the idea that if phase transition may occur in the Rh_2B, which may bring about novel properties. Detailed structural, mechanical, and electronic properties theoretical investigations of Rh_2B are also seldom. Are there compounds with higher boron contents?High boron compounds did not reveal any new phases so far. The results are worth making the effort.

In this article, we report two new phases for Rh_2B and RhB_2 by the first-principles calculations. Our results show that the predicted new phase of Rh_2B belongs to the monoclinic $P2_1/m$ phase, which is energetically much more stable than the previously proposed *Pnma* structure in experiments. At the pressure of about 39 GPa, the $P2_1/m$ phase transforms to $C2/m$ phases. While the structure type of the new phase of RhB_2 also belong to the monoclinic $P2_1/m$ phase. Both of the two phases are dynamically and mechanically stable at ambient pressure. Further calculations are performed to study the properties of those high-pressure phases.

Results and discussion

At ambient pressure, the variable cell simulation revealed a monoclinic Rh_2B-I ($P2_1/m$) structure as the most stable phase for Rh_2B, as shown in Fig. 1 (a). The $P2_1/m$ structure contains two Rh_2B f.u. in a unit cell (a = 5.615 Å, b = 2.873 Å, c = 4.715 Å, and β = 73.17 °), in which three inequivalent atoms Rh1, Rh2, and B occupy the Wyckoff 2*e* (0.928, 0.250, 0.769), 2*e* (0.561, 0.750, 0.230), and 2*e* (0.775, 0.250, 0.396) sites, respectively. Fig. 1 (b) along the y-axis and Fig. 1 (c) along the z-axis reveals a fundamental building block in the Rh_2B-I structure. For RhB_2, the predicted RhB_2-II ($P2_1/m$) is the most thermodynamically stable phase among the considered structures. Fig. 1 (d) shows the structure of RhB_2-II. RhB_2-II belongs to a monoclinic ($P2_1/m$) space group containing two RhB_2 f.u. in a unit cell (a = 6.044 Å, b = 3.057 Å, c = 6.116 Å and β = 100.72 °), in which Rh1, Rh2, B1, B2, B3 and B4 atoms occupy the Wyckoff 2*e* (0.306, 0.750, 0.043), 2*e* (0.292, 0.250, 0.448), 2*e* (0.015, 0.750, 0.397), 2*e* (0.963, 0.750, 0.086), 2*e* (0.582, 0.250, 0.279) and 2*e* (0.258, 0.250, 0.783) sites, respectively. From Fig. 1 (e) along the y-axis, it is seen that the boron atom sheets consist of triangle rings, within the triangle rings boron atom layer, the shortest B–B bond is 1.67 Å, which is smaller than the OsB_2 (1.87 Å). At the same time, the boron atoms form a three dimensional space grid structure in Fig. 1 (f), and avoid the happening of the interaction between metal atoms.

We calculated the formation enthalpy of the considered structural candidates of Rh_2B and RhB_2 in the pressure range of 0-100 GPa. The formation enthalpy of Rh_xB_y with respect to the pure phases is investigated by the following equations $\Delta H = H_{RhxBy} - xH_{Rh} - yH_B$. The Rh (space group: *Fm-3m*)[25] and

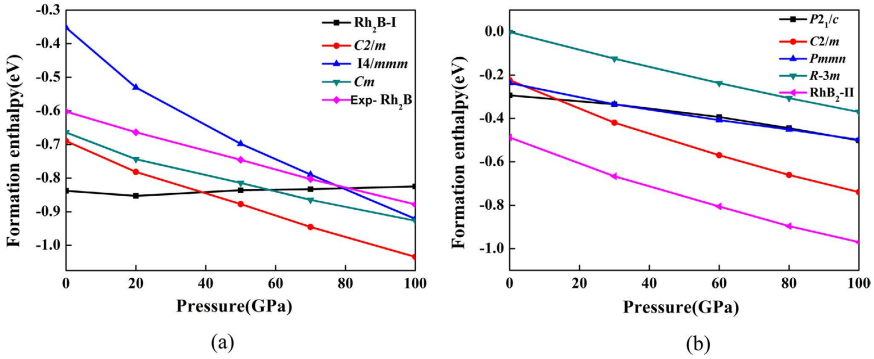

Figure 2. Formation enthalpy-pressure diagrams. Calculated enthalpies per unit of various structures relative to the (Rh + αB) as a function of pressure range from 0–100 GPa. (**a**) Rh_2B-I and (**b**) RhB_2-II

α-Boron (space group: *R*-3*m*)[26] were chosen as the referenced phases. Fig. 2 presents the enthalpy curves of Rh_2B and RhB_2 structure relative to the (Rh + αB) within the given pressure range. From Fig. 2, it can be clearly seen that the Rh_2B-I has the lowest negative formation enthalpies at ambient pressure, and the enthalpy of Rh_2B-I is much lower than that Rh_2B in experiment by ~0.16 eV per formula. This indicates that Rh_2B-I is thermodynamically stable and can be synthesized in experiments. When the pressure is higher than 39 GPa, the phase transition from $P2_1/m$ phase to C2/m phase, because C2/m phase is more energetically stable in high pressure. In experiment, they used high purity rhodium metal and relatively pure boron (98.8% with slight amounts of iron and carbon)[24]. They directly mix and sinter the samples for Rh_2B. The experimentally observed phase is a metastable phase with impurities. This can explain no presence of our predicted phases of Rh_2B in experiments. For RhB_2, the predicted RhB_2-II is the most thermodynamically stable phase in our calculations, no further phase transition was observed in the high pressure range.

To check the dynamical stabilities of the currently predicted Rh_2B-I and RhB_2-II, we have calculated their phonon dispersion curves. A stable crystalline structure requires all phonon frequencies to be positive, as seen in Fig. 3 (a,b), the absence of any imaginary phonon frequency in the whole Brillouin zone for Rh_2B-I and RhB_2-II indicate the dynamical stabilities of the two structures at ambient pressure. In Fig. 3 (c), the calculated phonon band structure shows no soft phonon, further confirming the stability of C2/m phase at 50 GPa.

Elastic constants are essential for understanding the mechanical properties of a crystal. We calculated the zero-pressure elastic constants C_{ij} of the two phases and the elastic constants C_{ij} are listed in Table 1. For a stable structure, C_{ij} has to satisfy Born–Huangcriteria[27]: For a monoclinic crystal, the independent elastic stiffness tensor consists of thirteen components of C_{11}, C_{22}, C_{33}, C_{44}, C_{55}, C_{66}, C_{12}, C_{13}, C_{23}, C_{15}, C_{25}, C_{35}, and C_{46}. The mechanical stability criteria is given by:

$$C_{11} > 0, C_{22} > 0, C_{33} > 0, C_{44} > 0, C_{55} > 0, C_{66} > 0$$

$$(C_{33}C_{55}–C_{35}^2) > 0, \ (C_{44}C_{66}–C_{46}^2) > 0, (C_{22} + C_{33}–2C_{23}) > 0$$

$$[C_{22}(C_{33}C_{55} - C_{35}^2) + 2C_{23}C_{25}C_{35} - C_{23}^2C_{55} - C_{25}^2C_{33}] > 0$$

$$g = C_{11}C_{22}C_{33} - C_{11}C_{23}^2 - C_{22}C_{13}^2 - C_{33}C_{12}^2 + 2C_{12}C_{13}C_{23}$$

$$\{2[C_{15}C_{25}(C_{33}C_{12} - C_{13}C_{23}) + C_{15}C_{35}(C_{22}C_{13} - C_{12}C_{33}) + C_{25}C_{35}(C_{11}C_{23} - C_{12}C_{13})] - [C^2{}_{15}(C_{22}C_{33} - C_{23}^2) + C^2{}_{25}(C_{11}C_{33} - C_{13}^2) + C_{35}^2(C_{11}C_{22} - C_{12}^2)] + C_{55}g\} > 0$$

As summarized in Table 1, the Rh_2B-I and RhB_2-II phases satisfy all mechanical stability criteria, indicating that they are mechanical stable at ambient pressure. The calculated C_{33} values are bigger than that of C_{11} and C_{22} in two structures, implying that the resistance to deformation along the *c*-direction is stronger than that along the *a*-direction and *b*-direction. The calculated bulk modulus of Rh_2B-I and RhB_2-II is 238 and 255 GPa, respectively, both phases can be grouped into incompressible materials. Besides the bulk modulus and shear modulus, Young's modulus could also provide a good measure of the stiffness of materials. The Young's modulus Y is obtained by the equation: Y = (9GB)/(3B + G). Young's modulus is defined as the ratio of stress and strain, and is used to provide a measure of the stiffness of materials in the range of elastic deformation. When the value of Y is large, the material is stiff[28]. The ratio value of *B*/*G* is commonly used to describe the ductility or brittleness of materials, with 1.75 as

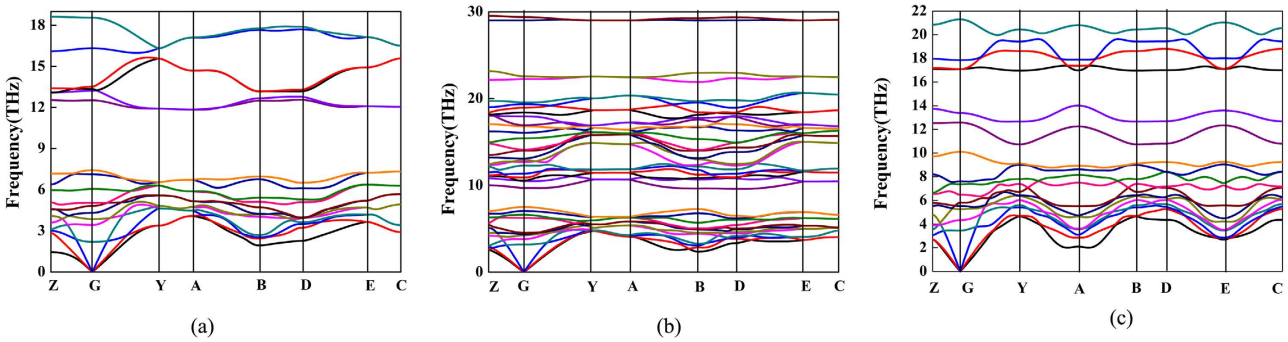

Figure 3. The phonon-dispersion curves. (**a**) Rh_2B-I at 0 GPa, (**b**) RhB_2-II at 0 GPa and (**c**) *C*2/m phase at 50 GPa respectively.

	C_{11}	C_{22}	C_{33}	C_{44}	C_{55}	C_{66}	C_{12}	C_{13}	C_{23}	C_{15}	C_{25}	C_{35}	C_{46}	*B*	*G*	*B*/*G*	*Y*	υ
Rh_2B-I	339	350	527	56	57	73	187	143	132	−2.45	−3.39	−0.74	−10.87	238	87	2.74	232	0.337
RhB_2-II	423	362	484	138	138	136	196	135	182	−80.74	4.28	−37.96	13.45	255	133	1.92	339	0.277

Table 1. Elastic Constants, Bulk Modulus (GPa), Shear Modulus (GPa), *B*/*G* ratio, Young's modulus Y (GPa), and Poisson's ratio υ of Rh_2B-I and RhB_2-II at zero pressure.

the critical value[29]. Higher (or lower) B/G value than the criteria indicates that the materials is ductile (or brittle). The *B*/*G* value of Rh_2B-I is 2.74, exceeding the critical value and implying its ductile nature. RhB_2-II also behaves in a ductile manner. The value of the Poisson's ratio υ is indicative of the degree of directionality of the covalent bonds. The Poisson's ratio υ is obtained by the equation: $\upsilon = (3B\text{-}2G)/2(3B + G)$. The typical υ value is 0.1 for covalent materials and 0.33 for metallic materials, respectively[30]. The Poission's ratio of RhB_2-II (0.277) is smaller than that of Rh_2B-I (0.377), indicating that the directionality degree of covalent bonding of RhB_2-II is stronger than that of Rh_2B-I. The directionality of covalent bonding plays an important role in the hardness of materials.

The electronic structure is crucial to the understanding of physical properties of materials. The electronic density of states (DOS) and the atom resolved partial density of states (PDOS) of the two phases at 0 GPa and *C*2/m phase at 50 GPa are shown in Fig. 4. In Fig. 4 (a), there is a deep valley at about −7 eV. It is a pseudogap of DOS, which is the borderline between the bonding and antibonding states. There are no clear overlap of rhodium's d electron and boron's p electron in range of −7 and 1 ev. In Fig. 4 (b) rhodium and boron atoms form strong covalent bonds as displayed by the much overlap of rhodium's *d* electron and boron's *s* electron, boron's *p* electron curves in comparison with that of Rh_2B-I. Indicating there is a strong covalent interaction between the B and Rh atoms in RhB_2-II. In Fig. 4 (c), there is a deep valley at about −9 eV. There are no clear overlap of rhodium's d electron and boron's p electron in range of −7 and 5 ev. The finite electronic DOS at the Fermi level indicates a metallic feature for the three phases.

To gain more detailed information about the bonding character, we calculated the electronic localization function (ELF) of Rh_2B-I , RhB_2-II at 0 GPa and *C*2/m phase at 50 GPa. The ELF was employed to understand the electron pairing and localization of the crystal structure. It should be noted that ELF is useful in distinguishing metallic, covalent, and ionic bonds[31]. The ELF is a contour plot in real space where different contours have values ranging from 0 to 1. ELF = 1 is that there is no chance of finding two electrons with the same spin. From Fig. 5, we can see clearly that the strong bonds between Rh and B in Rh_2B-I. This is consistent with the analysis of their DOS. The system of covalent bonds in the RhB_2-II is significantly anisotropic, where the neighbor boron atoms form very powerful covalent bonds within the planar triangle unit, whereas Rh–B bonds are appreciably weaker. Therefore, these strong covalent bonding will increase the structural stabilities and high bulk moduli of RhB_2-II. In Fig. 5(c) there are strong bonds between Rh and B in *C*2/m phase.

Conclusions

In summary, we have predicted a new phase Rh_2B-I at ambient pressure for Rh_2B and a new phase RhB_2-II for RhB_2 through the *ab initio* calculation. The two new phases all belong to monoclinic $P2_1/m$ structure. Besides, both of the two phases are dynamically and mechanically stable at ambient pressure. Rh_2B-I is energetically much superior to the previously proposed *Pnma* structure in the experiment. At the pressure of about 39 GPa, a phase transition occurs between the $P2_1/m$ and $C2/m$ phases for Rh_2B.

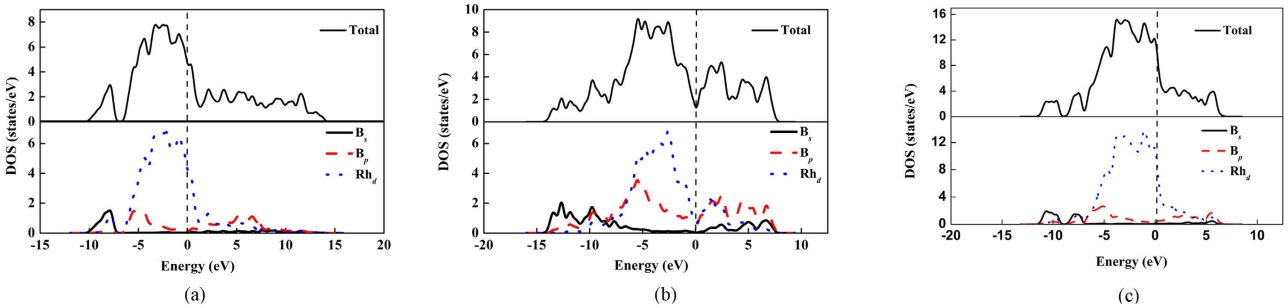

Figure 4. The total and partial densities of states. (**a**) Rh_2B-I phase at 0 GPa, (**b**) RhB_2-II phase at 0 GPa and (**c**) *C*2/m phase at 50 GPa respectively.

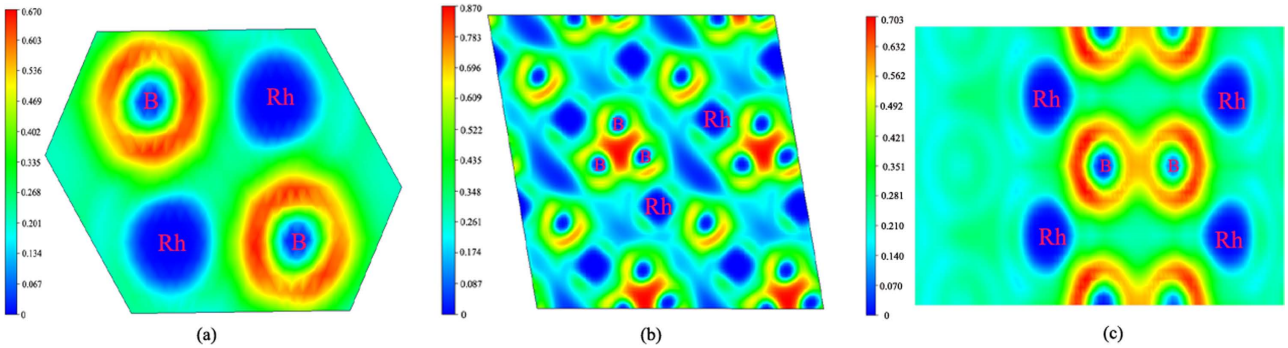

Figure 5. Contours of the electronic localization function (ELF). Electron localization function isosurface maps for (**a**) Rh_2B-I at 0 GPa, (**b**) RhB_2-II at 0 GPa, and (**c**) *C*2/m phase at 50 GPa respectively.

For RhB_2, RhB_2-II is the most thermodynamically stable phase in our calculations, no further phase transition was observed in the high pressure range.

Computation details. The evolutionary variable-cell simulations for Rh_2B and RhB_2 were performed at ambient pressure as implemented in the USPEX code[32–34]. The structure relaxation was performed by using the density functional theory implemented in the Vienna *ab initio* simulation package (VASP) code[35–37]. The exchange correlation functional was treated by the generalized gradient approximation (GGA)[38] with the projector-augmented wave (PAW) potential. The tested energy cutoff 450 eV was used, the *k*-points amplings in the Brillouin zone were performed using Monkhorst-Pack method (for the hexagonal structures, a Gamma-centered *k*-points was used) to ensure that enthalpy calculations are well converged with energy differences of less than 1meV/per atom. For each candidate structure, the atomic positions, bond lengths, and cell parameters were fully optimized. Elastic constants were carried out using the CASTEP code[39] and the bulk modulus, and shear modulus were thus estimated by using the Voigt-Reuss-Hill approximation[40]. The phonon calculations were carried out by using a supercell approach as implemented in the PHONON code[41]. The details of convergence tests have been described elsewhere[42–45].

References

1. Brazhkin, V. V., Lyapin, A. G. & Hemley, R. J. Harder than diamond: Dreams and reality. *Philos. Mag. A* **82,** 231–253 (2002).
2. Mounet, N. & Marzari, N. First-principles determination of the structural, vibrational and thermodynamic properties of diamond, graphite, and derivatives. *Phys. Rev. B* **71,** 205214 (2005).
3. Brazhkin, V. *et al.* From our readers: What does 'harder than diamond' mean. *Nat. Mater.* **3,** 576–577 (2004).
4. Zheng, J. C. Superhard hexagonal transition metal and its carbide and nitride: Os, OsC, and OsN. *Phys. Rev. B* **72,** 052105 (2005).
5. Solozhenko, V. L. *et al.* Ultimate Metastable Solubility of Boron in Diamond: Synthesis of Superhard Diamondlike BC_5. *Phys. Rev. L.* **102,** 015506 (2009).
6. Solozhenko, V. L. *et al.* Synthesis of superhard cubic BC_2N. *Appl. Phys. Lett.* **78.** 1385 (2001).
7. Kaner, R. B., Gilman, J. J. & Tolbert, S. H. Designing Superhard Materials. *Science* **308,** 1268–1269 (2005).
8. Ivanovskii, A. L. Mechanical and electronic properties of diborides of transition 3d–5d metals from first principles: Toward search of novel ultra-incompressible and superhard materials. *Prog. Mater. Sci.* **57,** 184–228 (2012).
9. Jonathan, B. L., Sarah, H. T. & Richard, B. K. Advancements in the Search for Superhard Ultra-Incompressible Metal Borides. *Adv. Funct. Mater.* **19,** 3519–3533 (2009).
10. Cumberland, R. W. *et al.* Osmium diboride, an ultra-incompressible, hard material. *J. Am. Chem. Soc.* **127,** 7264–7265 (2005).
11. Hao, X. F. *et al.* Low-compressibility and hard materials ReB_2 and WB_2: Prediction from first-principles study. *Phys. Rev. B* **74,** 224112 (2006).

12. Chung, H. Y. *et al.* Correlation between hardness and elastic moduli of the ultraincompressible transition metal diborides RuB_2, OsB_2, and ReB_2. *Appl. Phys.Lett.* **92,** 261904 (2008).
13. Zhao, Z. S. *et al.* Semiconducting Superhard Ruthenium Monocarbide. *J. Phys. Chem. C.* **114,** 9961–9964 (2010).
14. Zhang, M. G. *et al.* Structural Modifications and Mechanical Properties of Molybdenum Borides from First Principles. *J. Phys. Chem. C.* **114,** 6722–6725 (2010).
15. Chung, H. Y. *et al.* Synthesis of Ultra-Incompressible Superhard Rhenium Diboride at Ambient Pressure. *Science*. **316,** 436–439 (2007).
16. Chen, Z. Y. *et al.* Structural and electronic properties of OsB_2: A hard metallic material. *Phys. Rev. B* **74,** 012102 (2006).
17. Gu, Q. F. Krauss, G. & Steurer, W. Transition Metal Borides: Superhard versus Ultra-incompressible. *Adv. Mater*. **20,** 3620–3626 (2008).
18. Zhang, R. F. *et al.* Stability and Strength of Transition-Metal Tetraborides and Triborides. *Phys. Rev. B* **108,** 255502 (2012).
19. Gou, H. Y. *et al.* Unusual rigidity and ideal strength of CrB_4 and MnB_4. *Appl. Phys. Lett*. **100,** 111907 (2012).
20. Niu, H. Y. *et al.* Structure, bonding, and possible superhardness of CrB_4. *Phys. Rev. B* **85,** 144116 (2012).
21. Rau, J. V. & Latini, A. New Hard and Superhard Materials: $RhB_{1.1}$ and $IrB_{1.35}$. *Chem. Mater.* **21,** 1407–1409 (2009).
22. Latini, A. *et al.* Superhard Properties of Rhodium and Iridium Boride Films. *ACS Appl. Mater. Interfaces*. **2,** 581–587 (2010).
23. Wang, Q. Q. *et al.* Novel High-Pressure Phase of RhB: First-Principles Calculations. *J. Phys. Chem. C*, **115,** 19910–19915 (2011).
24. Mooney, R. W. & Welch, A. J. E. The crystal structure of Rh_2B. *Acta Crystallographica*. **7,** 49–53 (1954).
25. Moshopoulou, E. G. Structure of Ce_2RhIn_8: an example of complementary use of high-resolution neutron powder diffraction and reciprocal-space mapping to study complex materials. *Acta Crystallographica Section B*. **B62,** 173–189 (2006).
26. Oganov, A. R. *et al.* Ionic high-pressure form of elemental boron. *Nature*. **457,** 863–867 (2009).
27. Wu, Z. J. *et al.* Crystal structures and elastic properties of superhard IrN_2 and IrN_3 from first principles. *Phys. Rev. B* **76,** 054115 (2007).
28. Born, M. On the stability of crystal lattices. *IProc. Cambridge Philos. Soc*. **36,** 160 (1940).
29. Pugh, S. F. The London, Edinburgh, and Dublin Philosophical Magazine and Journal of Science: Series 7. *Philos. Mag.* **45,** 823–843 (1954).
30. Haines, J., Léger, J. M. & Bocquillon, G. Synthesis and design of superhard material Annu. *Rev. Mater. Res*. **31,** 1–23 (2001).
31. Savin, A. *et al.* On the Bonding in Carbosilanes. *Angew. Chem. Int. Ed. Engl*. **31,** 185–187 (1992).
32. Oganov, A. R. & Glass, C. W. Crystal structure prediction using ab initio evolutionary techniques: Principles and applications. *J. Chem. Phys*. **124,** 244704 (2006).
33. Oganov, A. R. Lyakhov, A. & Valle, O. M. *Acc. Chem. Res*. **44,** 227–237 (2011).
34. Lyakhov, A. O. *et al.* New developments in evolutionary structure prediction algorithm USPEX. *Comp. Phys. Comm*. **184,** 1172–1182 (2013).
35. Kresse, G. & Hafner, J. Ab initio molecular dynamics for liquid metals. *Phys. Rev. B* **47,** 558–561 (1993).
36. Kresse, G. & J. Hafner, J. Norm-conserving and ultrasoft pseudopotentials for first-row and transition elements. *Phys.: Condens. Matter* **6,** 8245 (1994).
37. Kresse, G. *et al.* Efficient iterative schemes for ab initio total-energy calculations using a plane-wave basis set. *Phys. Rev. B* **54,** 11169–11186 (1996).
38. Perdew, J. P. & Wang, Y. Accurate and simple analytic representation of the electron-gas correlation energy *Phys. Rev. B* **45,** 13244–13249 (1992).
39. Segall, M. D. *et al.* First-principles simulation: ideas, illustrations and the CASTEP code. *J. Phys. Condens. Matter*. **14,** 2717 (2002).
40. Hill, R. The Elastic Behaviour of a Crystalline Aggregate. *Proc. Phys. Soc*. **A65,** 349–354 (1952).
41. Parlinski, K. *Computer code PHONON*. <http://wolf.ifj.edu.pl/phonon/>.
42. Li, D. *et al.* Lowest enthalpy polymorph of cold-compressed graphite phase. *Phys. Chem. Chem. Phys*. **14,** 4347–4350 (2012).
43. Li, D. *et al.* Mechanical and metallic properties of tantalum nitrides from first-principles calculations. *RSC Adv*. **4,** 10133–10139 (2014).
44. Li, D. *et al.* Modulated T carbon-like carbon allotropes: an ab initio study. *RSC Adv*. **4,** 17364–17369 (2014).
45. Chu, B. H. *et al.* Ultrahard boron-rich tantalum boride: Monoclinic TaB_4. *J. Alloys Comp*. **617,** 660–664 (2014).

Acknowledgments

We are thankful for the financial support from the National Basic Research Program of China (No. 2011CB808200), Program for Changjiang Scholars and Innovative Research Team in University (No. IRT1132), National Natural Science Foundation of China (Nos. 51032001, 11074090, 11404134, 10979001, 51025206, 11104102, 11204100), and National Found for Fostering Talents of basic Science (No. J1103202), and China Postdoctoral Science Foundation (2014M561279, 2013T60314, 2012M511326). Specialized Research Fund for the Doctoral Program of Higher Education (20110061120007, 20120061120008). Parts of calculations were performed in the High Performance Computing Center (HPCC) of Jilin University

Author Contributions

T.C. initiated the project. B.C. performed the first principle calculations and prepared all figures. B.C., D.L., F.T., D.D., and T.C. analyzed the data and wrote the manuscript text. X.S., Y.L., H.Z., and B.L.reviewed the manuscript.

Additional Information

Competing financial interests: The authors declare no competing financial interests.

How to cite this article: Chu, B. *et al.* Structural, mechanical, and electronic properties of Rh2B and RhB2: first-principles calculations. *Sci. Rep.* **5**, 10500; doi: 10.1038/srep10500 (2015).